

Acoustic Journal Bearing with Changeable Geometry and Built-in Flexibility

T. A. Stolarski^{a)} and M. Miyatake^{b)}

^{a)} Brunel University London, Kingston Lane, Uxbridge, Middlesex UB8 3PH, United Kingdom
e-mail: mesttas@brunel.ac.uk

^{b)} Tokyo University of Science, 6-3-1, Nijjuku, Katsushika-ku, Tokyo 125-8585, Japan
e-mail: m-miyatake@rs.tus.ac.jp

Abstract

The influence of embodiment flexibility on the performance of an acoustic journal bearing is presented. Two completely different embodiments of the bearing were investigated using three criteria of performance assessment that is torque at the start-up, amount of separation due to squeeze film pressure and motion stability of the shaft running at speed. The embodiment with built-in flexibility proved to perform far better than the bearing which overall flexibility was much less. However, considerations pertinent to the ease of machining and fatigue endurance mitigate the ranking of performance of the two embodiments investigated.

Keywords: Journal air bearing; squeeze-film; acoustic levitation; bearing's embodiment; elastic deformation; precision of motion

1. Introduction

1.1 Scope and aims

The full separation of contacting surfaces is fundamental to the operation of precision mechanical systems. For making accurate industrial products in micro-fabrication and nanotechnology contexts, such as semiconductor silicon wafers, micro-components and integrated circuits, non-contact, oil-free, ultra-precision and low wear transport along the production line is crucial and urgent [1].

Traditional methods of separating contacting surfaces, such as rolling, and oil-based sliding contacts are simply unsuitable for applications requiring "clean room" operating conditions and high precision of motion. This is especially true for food, drug, and semiconductor industries together with medical and biomedical equipment. Also, traditional ways of securing separation of interacting surfaces cannot be used in many ultra-precision devices where extreme accuracy of motion, in the order of nanometres, is required. Laser scanner motors, hard disc drives, and contact-less transportation of silicon chips in lithography process are examples of industries calling for a new class of bearings.

Although alternatives to traditional bearings are available now in the form of aerostatic and magnetic bearings, however, both techniques are prone to operational difficulties. For instance, aerostatic bearings separate surfaces using a thin layer of pressurised gas and so require auxiliary equipment, which may cause considerable practical difficulties especially where space is at premium [2]. Magnetic bearing technology has been available for about 25 years and utilises an active magnetic field of appropriate density. Although magnetic bearings may be suitable for many special applications, however, practical problems related to the

complexity of their design and the lack of complete reliability, a backup system is usually required for some applications, have considerably restricted the growth of magnetic bearing technology. Also, active magnetic field is a potential health hazard and may interfere with the operation of other systems and devices located in close proximity. Finally, magnetic bearings require some sort of feedback control for stable operation [3].

A potential solution to the problems identified with current ultra-precision bearing technology is offered by this paper. The solution is based on a new idea and represents a radical departure from the current bearing technology. It utilises acoustic levitation, which relies on the sound energy radiated by an object to support, or levitate, an object. In order to support a load the acoustic wave emitted by the radiating surface must be reflected back towards the radiating surface by the levitating object. The radiation pressure increases as the gap between the sound source and levitating objects narrows. This phenomenon is commonly known as near field acoustic levitation (NFAL) and has the potential to support loads equivalent to those found in many magnetic and aerostatic applications.

Journal bearing configuration appears to be well suited to the application of NFAL as it is likely that high radiation sound pressures may readily be generated between the bearing shell and journal. Although NFAL has a potential to separate the journal from bearing shell, however, it might not secure stable and accurate motion of the journal, which is especially important for high-speed and high-precision applications. For that reason, the geometry of the bearing proposed can be changed in order to stabilise the journal motion if required. This is achieved by elastically deforming the circular bore of the bearing in order to obtain geometry required for dynamic stability even at very high rotational speeds.

Squeeze-film levitation (SFL) occurs when a flat item is located adjacent to a vibrating structure. Accordingly, as a result of the surrounding air viscosity and compressibility, a thin film of air (squeeze-film) is trapped with average pressure greater than the atmospheric pressure producing a load supporting force.

In both mechanisms, geometry and flexibility of the bearing's shell is important and is the prime topic of this paper.

1.2 Physical fundamentals of the acoustic bearing operation

Langlois [4] was one of the first to demonstrate that the squeeze-film levitation mechanism can be practically utilised for gas film bearings. Hashimoto et al [5] examined the NFAL to assess its dynamic performance. Matsuo et al [6] appraised functioning of the levitation force applied to an object to be floated using NFAL method. They found that the levitation force strongly depends on the oscillation frequency of the surface emitting sound. Ueha et al [7] created a contact free displacement of an object employing bespoke device including piezo-electric transducers (PZTs) operating in ultrasonic domain. Minikes et al [8] studied both theoretically and experimentally the dynamic performances of a levitating object due to the action of ultrasonic PZTs. They assumed in their examinations that the squeeze-film action is the main operating mechanism represented by the spring and damper elements and controlled by the oscillation frequency. Nomura et al [9] explored NFAL aiming at establishing sound understanding of its fundamental mechanism. The study consisted in using an ultrasonic PZT attached to disks made of aluminium to demonstrate the floating characteristics. Hu et al [10] investigated the permanency of a levitating disk placed on an oscillating transducer. Foresti et al [11] explored in their studies the effect of geometry on NFAL and concluded that the resonance frequency of a radiator plate is not affected by its

motion resulting from elastic deformations. Stolarski and Woolliscroft [12] explored levitation of lightweight objects floating over a plate with PZTs attached to it. The investigation confirmed that levitation was primarily due to the SFL mechanism and floating height of an object was mainly affected by the location of PZTs on the plate. Wang et al [13] investigated the SFL characteristics of a disc subjected to ultrasonic oscillations and resulting from its modal shapes. Disc's modal shapes creating levitation were determined. An analytical model describing dynamics of objects levitating due to NFAL was put forward by Ilssar and Bucher [14]. The subsequent studies by Ilssar et al [15] improved efficiency of the levitation process and contributed to increasing accuracy required by high precision positioning in micro fabrication. Chang et al [16] constructed a device containing a plate subjected to vibration produced by round type PZTs attached to it. They demonstrated that modal shapes together with harmonic shapes play an important role in resulting levitation parameters. Wei et al [17], exploiting an inverse aerodynamic principle applicable to a squeeze film mechanism operating in skewed surfaces, designed a working device capable of inducing levitation.

2. Concept of the squeeze-film acoustic levitation bearing

Figure 1 shows, schematically, the essence of the squeeze film mechanism.

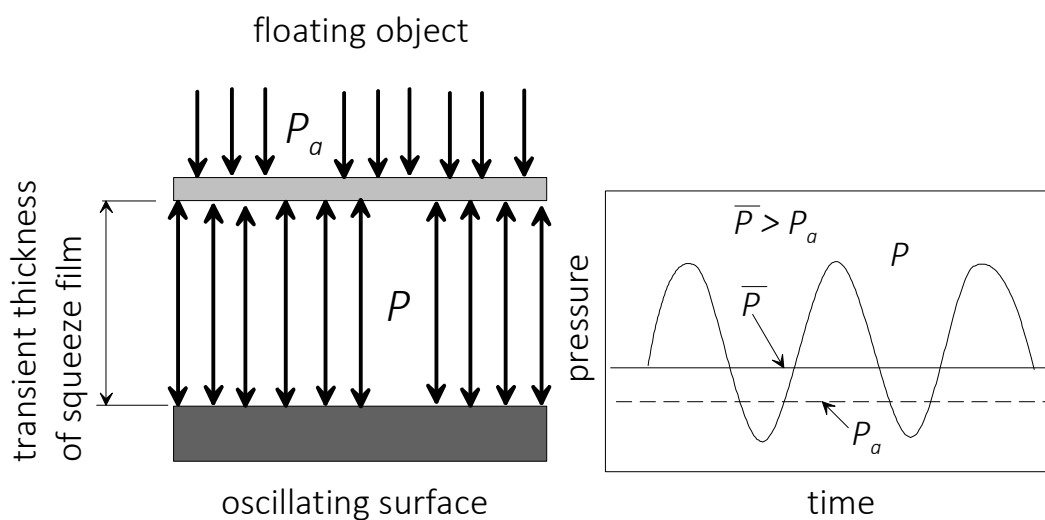


Figure 1

Essence of the squeeze film mechanism

P – oscillating pressure (transient); P_a – ambient pressure; \bar{P} – resulting pressure

Due to oscillatory motion of one of the surfaces, separated by a thin air film, an average positive pressure greater than ambient pressure is generated within the film and an object can float. This fundamental mechanism of squeeze film pressure generation is based on Bernoulli principle and its details can be found elsewhere [18]. To use this physically sound principle in the context of a journal bearing geometry and configuration it is necessary to create an appropriate geometry of the bearing shell. This can be achieved by elastically

deforming circular bearing shell into a geometry resembling, for instance, a well-known 3-lobe configuration as shown in Figure 2. By oscillating the bearing shell with prescribed frequency it is possible to reproduce the situation shown in Figure 1. The practical way to achieve that is to utilize piezoelectric transducer (PZT) – a device commonly used in engineering systems. One possible configuration of a bearing with attached to it PZTs is shown in Figure 3. Under the action of 3 PZTs attached to the bearing its shell deforms elastically creating three-lobe geometry within the bearing clearance. Periodic oscillations of the shell with prescribed amplitude and

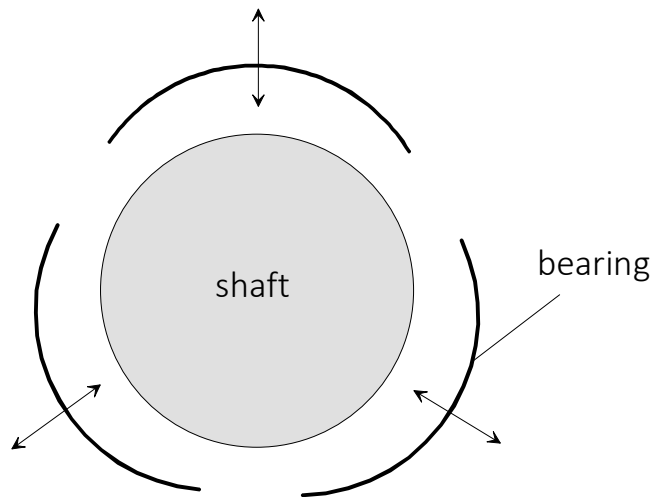


Figure 2

Schematic showing geometry of elastically deformed bearing.

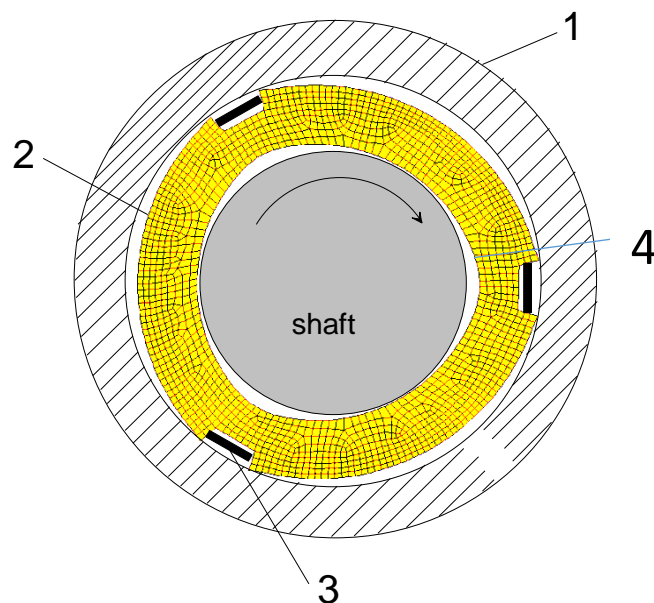


Figure 3

Bearing in a deformed state: 1 – housing, 2 – bearing shell, 3 – PZT, 4 – oscillating “half-moon” gap

frequency should, in accordance with the squeeze-film mechanism, generate a pressure within lubricating air film.

3. Analytical model

The concept of the bearing implies that its geometry will be cyclically changing thus giving rise to a squeeze film action. Figure 4 depicts position of the shaft relative to the bearing shell. Also shown are vital parameters of the bearing required to build an analytical model of it.

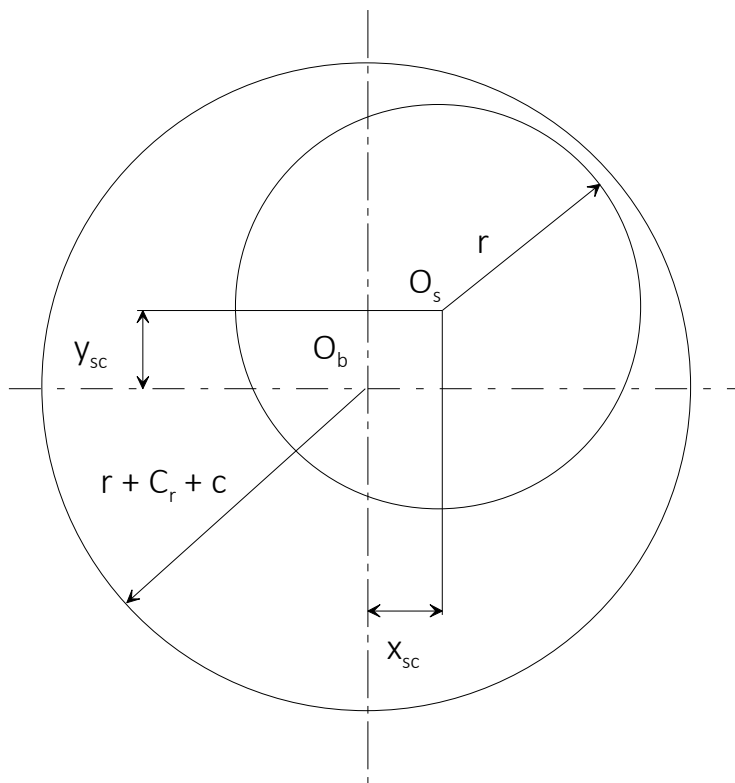


Figure 4

Diagram of bearing system for its analytical model.

In order to create computer model of the journal bearing operating on squeeze film ultrasonic levitation it is necessary to insert into the Reynolds' equation time dependent term. Integration of the continuity equation across the thin air film leads to a differential form of the Reynolds' equation.

$$\frac{\partial q_x}{\partial x} + \frac{\partial q_y}{\partial y} + \frac{\partial(\rho h)}{\partial t} = 0 \quad (1)$$

In the above equation, symbols q_x and q_y denote mass flow rates per unit length. Taking into account geometry shown in Figure 4, the equation for the thickness of air film can be expressed as:

$$h = C_r + x_{sc}\sin\theta + y_{sc}\cos\theta + c(\theta, z, t) \quad (2)$$

The last term in the expression for air film thickness on its right-hand side is a contribution resulting from cyclic elastic deformation of the bearing's bore. More generally, this term can be written as,

$$c(\theta, z, t) = A \times B \times \sin(2\pi ft) \quad (3)$$

Values for A and B in the above equation were arrived at using experimentally measured deformation of the bearing shell for a given voltage applied to three PZTs located as shown in Figure 3.

Introduction of non-dimensional variables gives,

$$h = C_r H$$

$$x_{sc} = X_{sc} C_r$$

$$y_{sc} = Y_{sc} C_r$$

$$z = r_0 Z$$

$$c = C C_r$$

Now, the non-dimensional equation for air film thickness assumes the form,

$$H = 1 + X_{sc}\sin\theta + Y_{sc}\cos\theta + C(\theta, Z, \tau) \quad (4)$$

Introducing polar co-ordinate system, mass flow rates incorporated in the Reynolds' equation adopt the following form,

$$q_\theta = \left(-\frac{h^3}{12\eta RT} \frac{p}{r_0} \frac{\partial p}{\partial \theta} + \frac{r_0 \omega_1}{2} \frac{p}{RT} h \right) \Delta z$$

$$q_z = \left(-\frac{h^3}{12\eta RT} p \frac{\partial p}{\partial z} \right) r_0 \Delta \theta$$

$$q_t = \frac{1}{RT} \frac{\partial(ph)}{\partial t} r_0 \Delta \theta \Delta z$$

After introduction of non-dimensional variables,

$$h = C_r H$$

$$p = p_a P$$

$$z = r_0 Z$$

$$t = \tau / \omega_2$$

expressions for mass flow rates look as shown below:

$$q_{\theta} = \frac{p_a^2 C_r^3}{12\eta RT} \left(-PH^3 \frac{\partial P}{\partial \theta} + \Lambda_1 PH \right) \Delta Z$$

$$q_z = \frac{p_a^2 C_r^3}{12\eta RT} \left(-PH^3 \frac{\partial P}{\partial Z} \right) \Delta \theta$$

$$q_t = \frac{p_a^2 C_r^3}{12\eta RT} \left(\sigma \frac{\partial(PH)}{\partial \tau} \right) \Delta \theta \Delta Z$$

In the above non-dimensional expressions for mass flow rates,

$$\Lambda_1 = \frac{6\eta r_0^2 \omega_1}{p_a C_r^2}$$

$$\sigma = \frac{12\eta r_0^2 \omega_2}{p_a C_r^2}$$

An important task in modelling is to derive expressions describing motion of the shaft's centre. Using non-linear orbit method, motion of the shaft's centre in two mutually perpendicular directions can be analytically described as,

$$m \frac{d^2 x_{sc}}{dt^2} = r_0 \int_0^b \int_0^{2\pi} p \cos \theta d\theta dz \quad (5)$$

$$m \frac{d^2 y_{sc}}{dt^2} = r_0 \int_0^b \int_0^{2\pi} p \sin \theta d\theta dz + f_y \quad (6)$$

where $f_y = mg \sin \phi$ is the force applied to the shaft.

Again, introducing non-dimensional notation, equations describing shaft's motion assume the form,

$$M \frac{d^2 X_{sc}}{d\tau^2} = \frac{r_0}{2b} \int_0^{b/r_0} \int_0^{2\pi} P \cos \theta d\theta dZ \quad (7)$$

$$M \frac{d^2 Y_{sc}}{d\tau^2} = \frac{r_0}{2b} \int_0^{b/r_0} \int_0^{2\pi} P \sin \theta d\theta dZ + F_y \quad (8)$$

Where,

$$F_y = \frac{f_y}{2p_a b r_0}$$

denotes the non-dimensional force applied to the shaft.

The above two equations describing the motion of the shaft within the bearing were solved using the Crank-Nicolson numerical procedure. Assuming continuity of flow over a unit domain and utilising the finite difference method, it is possible to predict pressure distribution within the air film.

4. Embodiments of the bearing

4.1 Embodiment with changeable geometry only

Embodiment of the bearing able to change its geometry under the action of PZTs is shown in Figure 5 as a photograph of actual bearing tested. Dimensions of the bearing are given in Table 1.

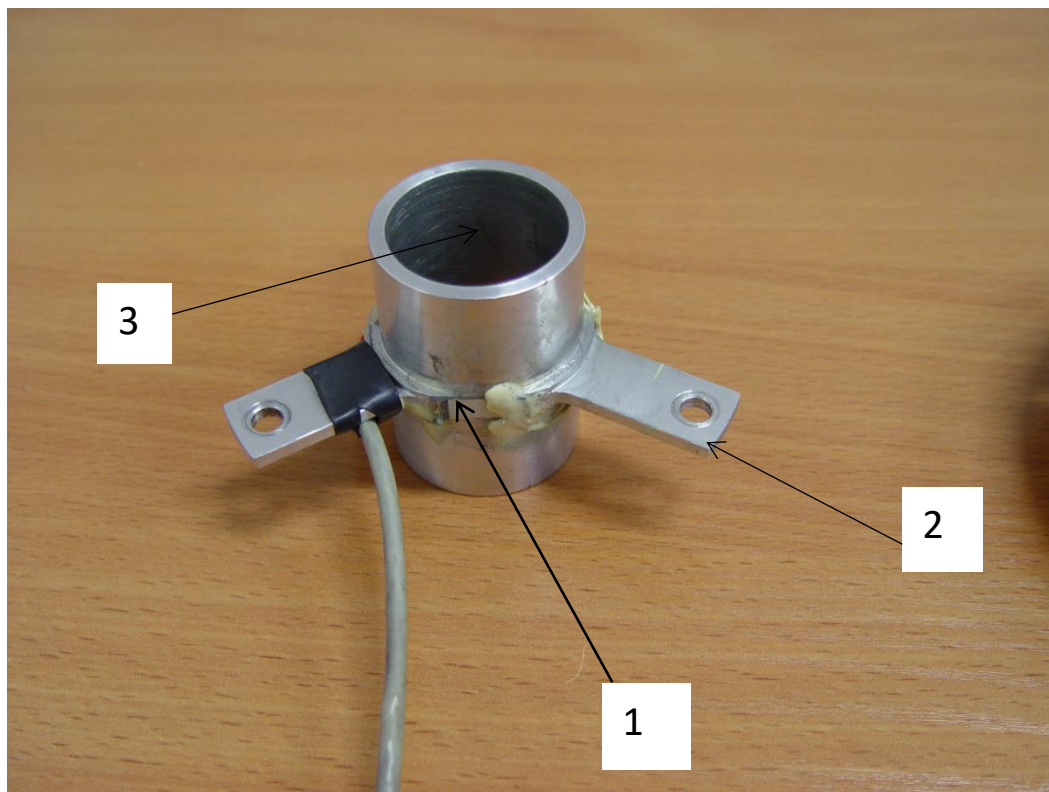


Figure 5

Photograph showing the first embodiment of the bearing.

1 – PZT (there are three PZTs spaced by 120 deg.); 2 – supporting and constraining arm fixing the bearing to its housing; 3 – inner surface of the bearing shell.

As it can be seen (Figure 5) the shape of the bearing is relatively simple therefore there were no special problems with its machining. It was made of an aluminium alloy because this material is characterised by a low coefficient of elastic strain energy absorption. At the locations indicated in Figure 5 three PZTs of the foil type were attached. Dimension of the PZTs used were: length – 12 mm, width – 10 mm and thickness – 0.5 mm. Under the action of PZTs, the bearing changed its geometry as shown in Figure 6. Solid 226 elements in ANSYS analysis were used. In modelling elastic deformation of the bearing due to action of PZTs contact elements were used to transmit the force generated by the PZT to the bearing structure. The offset voltage was 60 V and the amplitude voltage 95 V. The first observation to be made is that the geometry of deformed bearing looks like well-known three lobe configuration frequently used to ensure dynamic stability of lightly loaded conventional air journal bearings. The second observation is that elastic deformation of the bearing bore is relatively small and equal to $0.123 \mu\text{m}$ for the applied offset voltage of 60 V.

This is because this embodiment is quite rigid and therefore significantly affected running performance of the bearing.

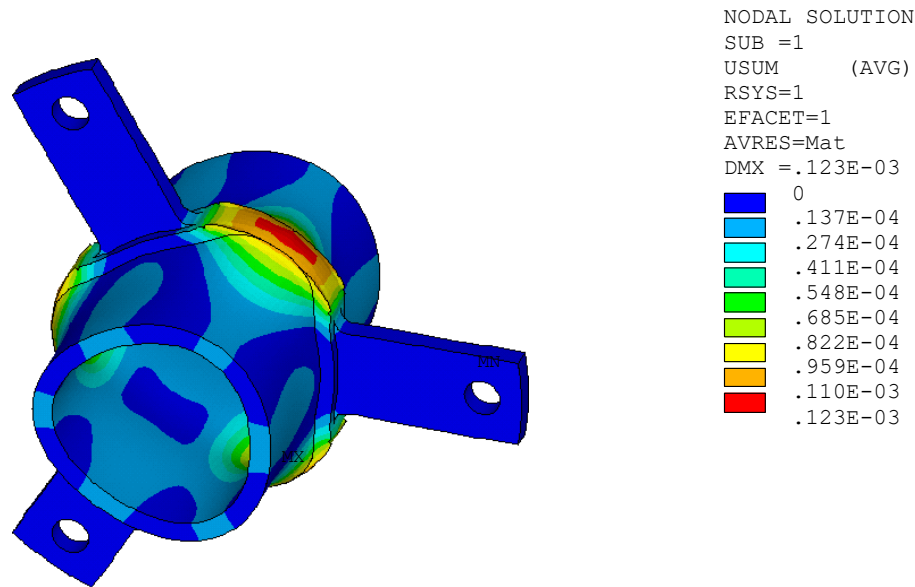


Figure 6

Image of the bearing (first embodiment) showing its deformation when applied offset voltage to PZTs was 60 V.

4.2 Embodiment with changeable geometry and built-in flexibility

Figure 7 is a photograph of the bearing with second embodiment and experimentally examined. As it can be seen the overall geometry and shape are completely different comparing with the first embodiment (see Figure 5). It can, as the bearing in its first embodiment, change its bore geometry but additionally is able to deform elastically much more. Dimensions of this bearing are given in Table 1. Due to the presence of “elastic hinges” (see Figure 7), which radically increased the overall flexibility of the bearing, a stainless steel was used for its machining. This was because of a concern that mechanically weaker material, like aluminium alloy, could fail due to fatigue at the location of elastic hinges. With stainless steel as a material of the bearing it was necessary to employ PZTs with stronger output comparing to the foil type used for the first embodiment. Therefore, three PZTs in a form of a rod with square cross-section 5x5 mm and length of 18 mm were installed at location indicated in Figure 7. In case of rod type PZT, a force generated at a given voltage was applied as a pressure to the bearing structure, therefore there was no need to use special elements model this type of PZTs in ANSYS analyses. The offset voltage was 95 V and amplitude voltage 110 V.

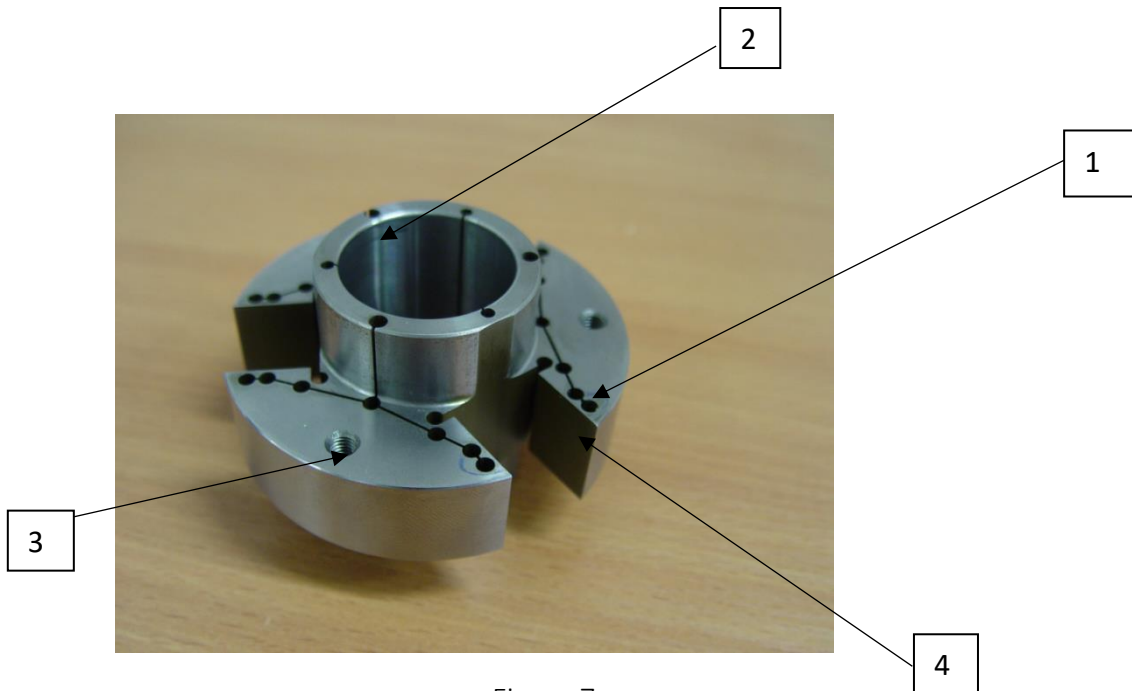


Figure 7

Photograph of the bearing in its second embodiment.

- 1- elastic hinge; 2 – bearing’s inner surface; 3 – outer surface totally constrained in the housing; 4 – slot for rod type PZT.

Bearing of the second embodiment in a deformed shape is shown in Figure 8. Elastic deformation of the bore is around $1.6 \mu\text{m}$ under the offset voltage of 95 V. It can easily be noticed that the bore assumes a three lobe configuration and the magnitude of elastic deformation is vastly greater than that achieved for the first embodiment. Experimental testing results, introduced later on, will demonstrate that the amount of elastic deformation of the bore is an important factor in squeeze film acoustic levitation mechanism on which operation of the bearing presented in this paper crucially depends on.

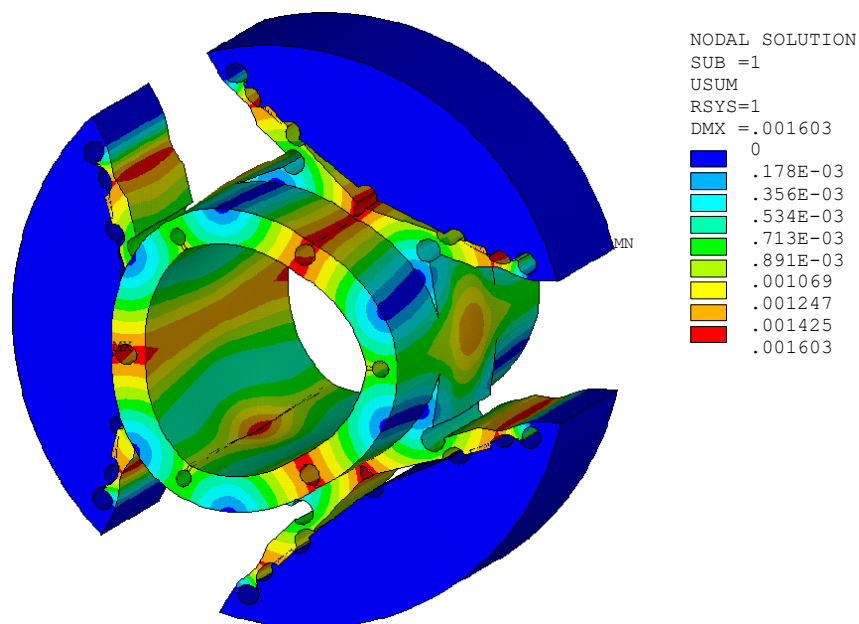


Figure 8

Image of the bearing (second embodiment) showing its deformation when applied offset voltage to PZTs was 95 V.

Table 1. Dimensional specification of tested bearings

Bearing embodiment	Nominal diameter [mm]	Length [mm]	Radial clearance [mm]
First embodiment	30	50	20×10^{-3}
Second embodiment	30	50	20×10^{-3}

5. Experimental testing arrangements

5.1 Test apparatus

The ultimate proof of the importance played by the flexibility of the acoustic bearing's embodiment can only be arrived at through experimental testing. Therefore, a purposefully designed testing apparatus was used to find out what influence on bearing's performance could have its embodiment flexibility or in other words its ability to deform in an elastic manner. Figure 9a shows schematic diagram depicting principle of its operation while Figures 9b, c, and d, are photographs of actual apparatus together with associated instrumentation and auxiliary equipment.

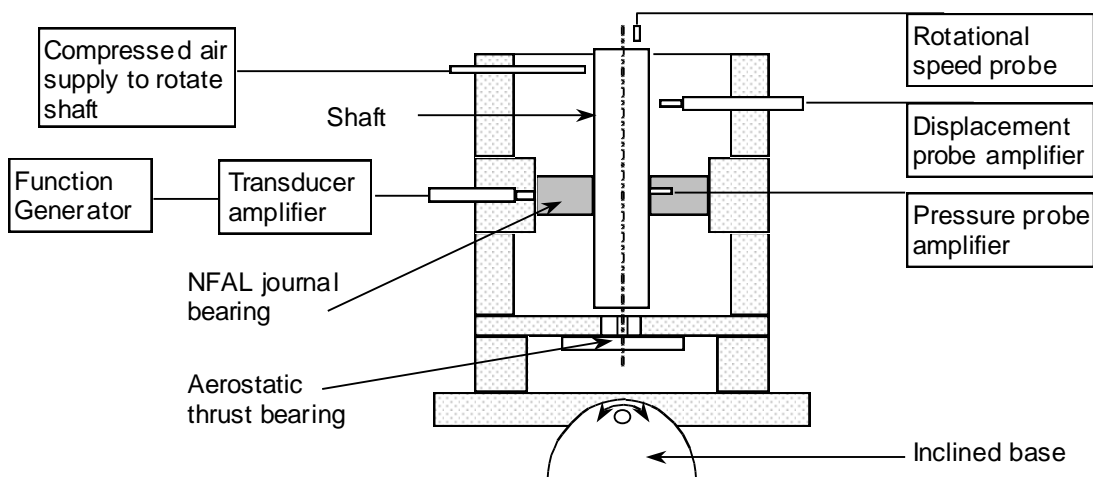


Figure 9a

Schematic of experimental apparatus.

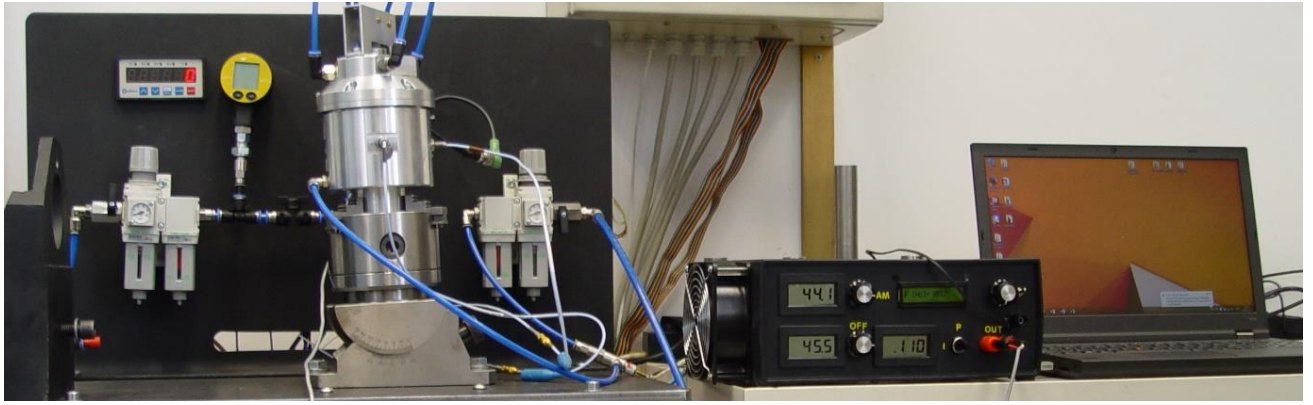


Figure 9b

Photograph showing experimental set-up.

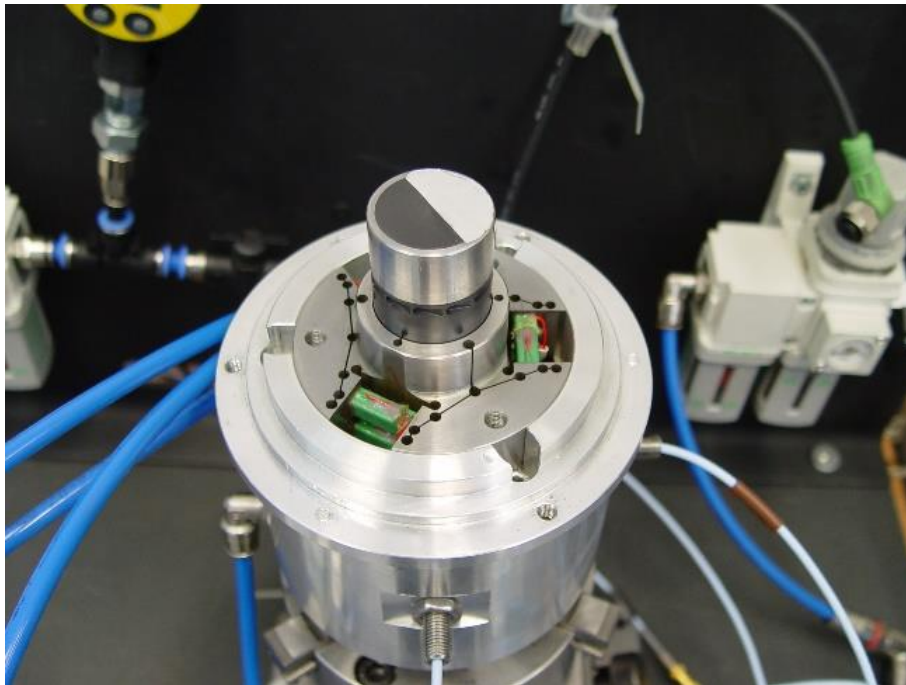


Figure 9c

Photograph showing top part of the apparatus. Rod type PZTs, shaft, and test bearing (second embodiment) are visible.

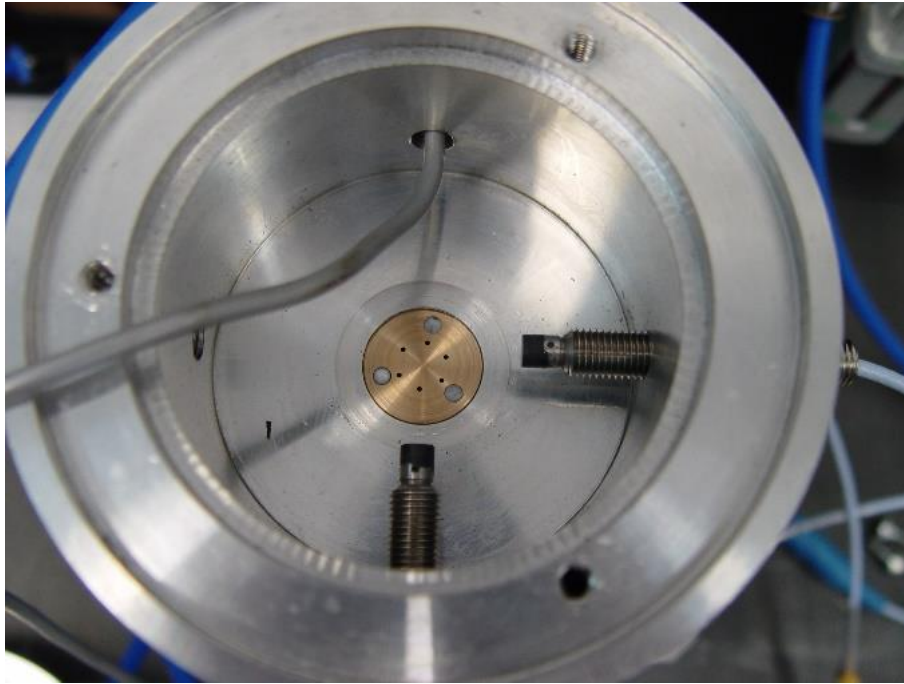


Figure 9d

Photograph showing aerostatic thrust bearing of the apparatus together with displacement probes monitoring shaft's motion.

A characteristic feature of the apparatus is a vertical position of the shaft and its tilting base. An aerostatic thrust bearing located at the bottom of the housing provides support for the shaft. The tested acoustic bearing was positioned half way through the length of the shaft and its geometric centre coincided with the mass centre of the shaft. The shaft, made of a stainless steel, had a nominal diameter of 30 mm. At the top of the shaft circumferentially machined buckets were used to rotate the shaft at speed. Compressed air was directed at the bucket tangentially to the shaft circumference by three nozzles attached to the housing. This arrangement of air nozzles resulted in a pure torque being applied to the shaft. Tilting of the apparatus in a controlled way facilitated application of the load on tested bearing. The load on the bearing was always acting between two adjacent PZTs and that was ensured by appropriate positioning of the bearing within its housing. This is schematically illustrated in Figure 10 which also gives the orientation of x-y axes relative to PZTs attached to the bearing.

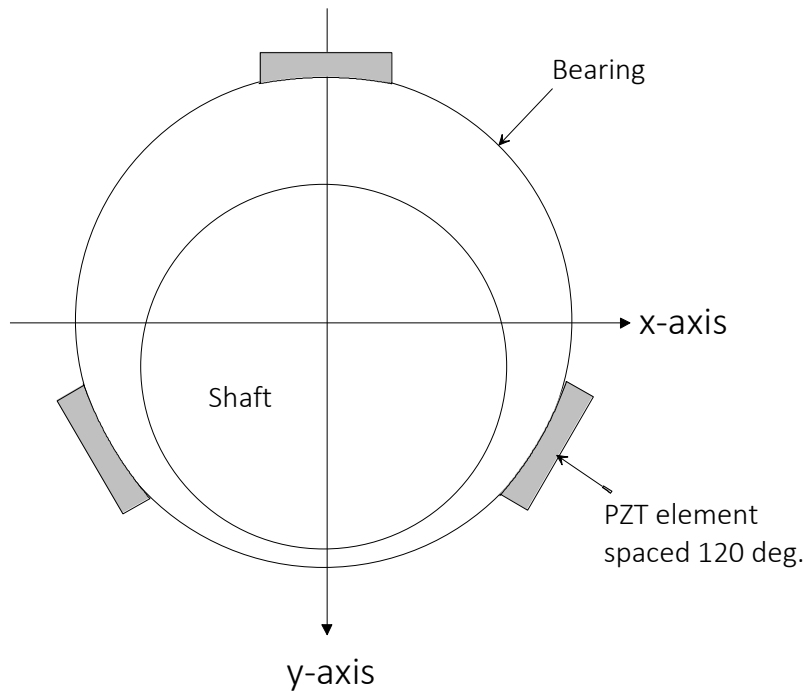


Figure 10

Schematic illustrating orientation of X and Y axes relative to PZTs. The load on the bearing acts along y-axis that is between two adjacent PZTs.

The magnitude of the load on the bearing was determined as a component of the shaft's weight corresponding to a given tilt angle of the apparatus. Experimental set up consisted of power supply unit powering PZTs, amplifier and frequency generator. Two contactless sensors, positioned at mutually perpendicular planes, were used to measure position of the shaft relative to the bearing centre. Also, a photocell located at the top of the apparatus provided information on rotational speed of the shaft.

5.2 Testing procedure

All tests were carried out using the same procedure which can be outlined as follows.

- (1) Vertical shaft position was checked and if necessary corrected by adjusting the base of the apparatus.
- (2) Offset voltage was set to required magnitude.
- (3) Amplitude voltage applied to create cyclic elastic deformation of the bearing's bore via PZTs.
- (4) Required rotational speed of the shaft attained when it was in a vertical position.
- (5) The apparatus was tilted by an angle to achieve required load on the test bearing.
- (6) With set rotational speed and load the dynamic behaviour of the shaft was observed and recorded with contactless probes positioned in mutually perpendicular directions.

(7) Recording of the shaft's position for a set speed and load in real time was accomplished with data acquisition system.

(8) Identical tests were carried out with PZTs switched on and when PZTs were switched off giving ample data for comparison of dynamic performance for these two testing set-ups.

6. Results and their discussion

6.1 Separation between shaft and bearing

Measurements of separation of the shaft from the bearing surface for two embodiments of the bearing were carried out for the case of stationary shaft using a contactless probe. A number of repeated measurements were implemented and estimated error was within $\pm 10\%$. Figure 11 shows the results where the vertical axis represents the distance between the shaft and the bearing at a given load denoted by the horizontal axis. All measurements were carried out at the frequency of bearing shell elastic deformations (case of PZTs switched on) equal to 58.3 kHz and the nominal radial clearance of 20 μm .

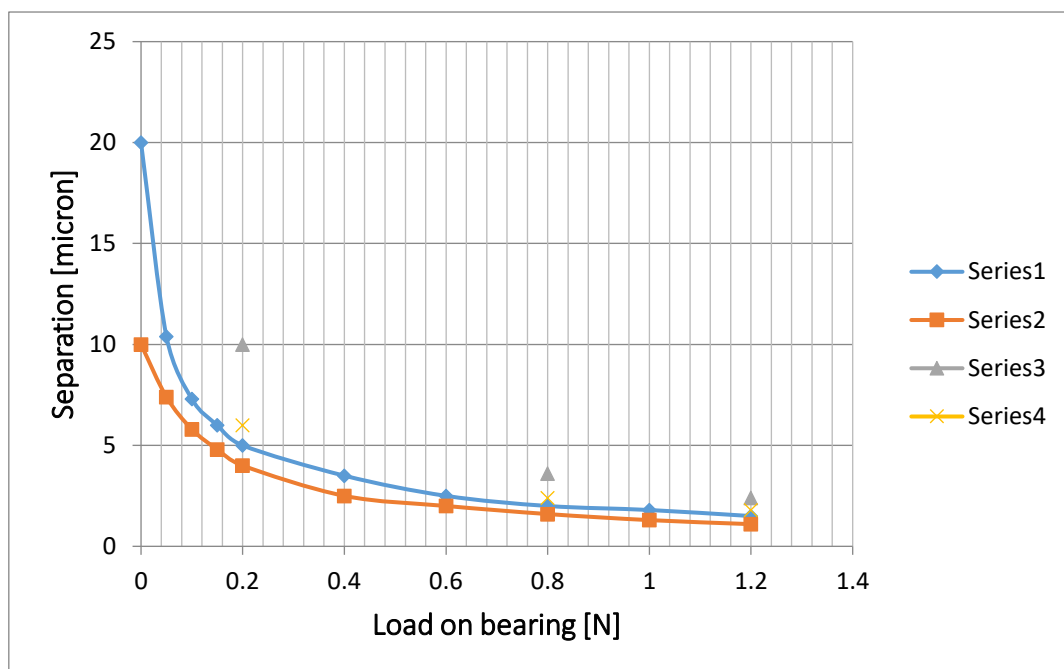


Figure 11

Separation of the shaft from inner bearing surface as a function of applied load. Series 1 – calculated separation for the second embodiment; Series 2 – calculated separation for the first embodiment; Series 3 – measured separation for the first embodiment; Series 4 – measured separation for the second embodiment.

In Figure 11 experimental results are plotted together with the results of calculations attained in accordance with equations introduced earlier. It can be seen that both

embodiments are able to support load of up to 1.2 N. However, the separation at this load is very small and practically negligible. Also, a reasonable agreement between measured and calculated separation can be observed, although measured separations are consistently greater than those calculated. This is presumably a reflection of the simplification assumed in the analytical model of the bearing.

Experimental results of measured separation between the shaft and bearing, shown in Figure 11, were additionally supplemented by the measured resistance to initiate motion of the shaft. Measuring the torque required to initiate shaft's motion provide indirect but useful information of the nature of the contact within the bearing. With low value of a torque required to initiate motion one can justifiably concluded that the shaft is separated from bearing's surface by a thin air film hence no direct contact and low resistance to motion. On the other hand high value of the resistance to initiate motion of the shaft usually indicates that there is a direct contact of the shaft with bearing's surface. Experimental measurements of this type are shown in Figures 12 and 13.

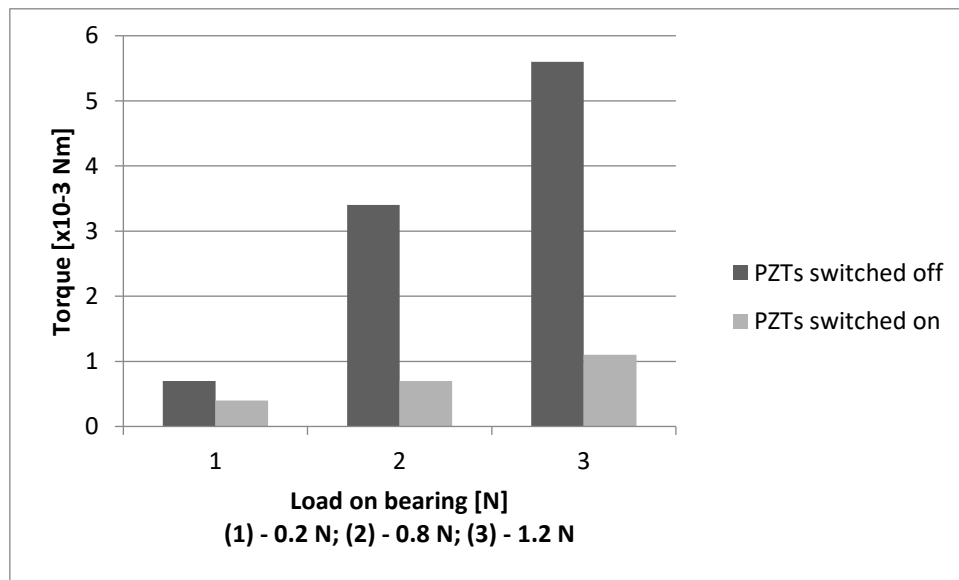


Figure 12

Torque required to start-up motion of the shaft for different loads (first embodiment).

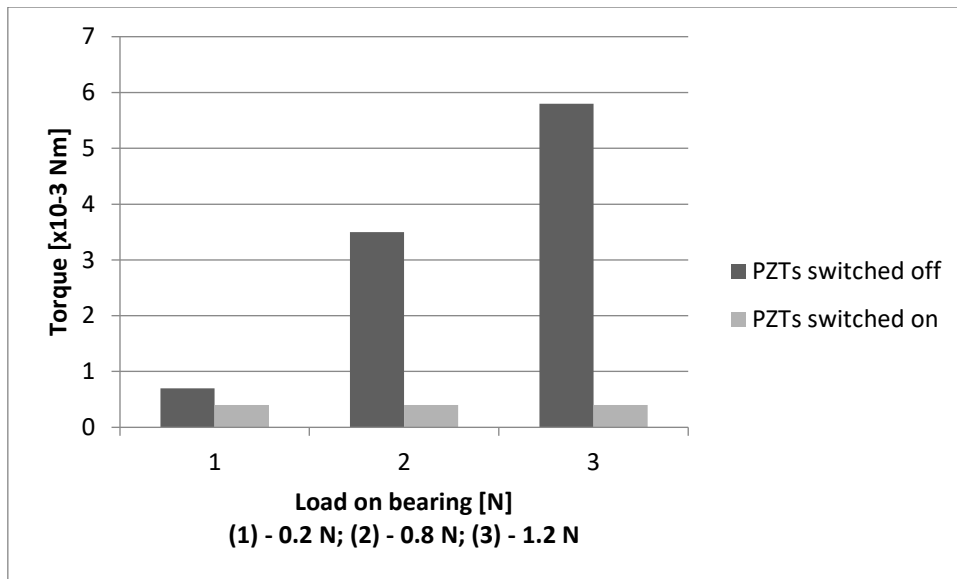


Figure 13

Torque required to start-up motion of the shaft for different loads (second embodiment).

Based on a few repeated measurements it was estimated that the error is within ± 5 . In Figure 12 presents results for the first embodiment of the bearing characterised by changeable geometry only while Figure 13 shows the results for the second embodiment of the bearing having both changeable geometry and, additionally, enhanced flexibility. Looking together at Figures 11, 12, and 13 one can conclude that there is a quite good qualitative agreement in support of what is happening within the bearing when the PZTs are switch on and when they are switched off.

The above findings have some important ramifications of a more generic nature. They show that an acoustic journal bearing operating on the squeeze film principle can support loaded shaft in a complete separation from the bearing during the start-up phase of its operation.

6.2 Motion stability of the shaft running at speed

When acoustic journal bearing runs at speed its operation is a kind of cooperation between squeeze film pressure and aerodynamic pressure generated when an appropriate rotational speed is attained. The effectiveness of the squeeze film pressure created when PZTs are switched on in stabilising the operation of a lightly loaded air bearing (known to be prone to a dynamic instability) is demonstrated and quantitatively measured here by the stability coefficient, S . This coefficient results from the ratio of maximum displacement of the shaft when it runs at speed for the bearing with PZTs switched on to the maximum displacement of the shaft running at the same speed but for the case of PZTs being switched off. Quantitative values of coefficient S , calculated separately for displacements in X direction and Y direction, were based data recorded by contactless probes. Displacements of the shaft were recorded for six different but relatively light loads on the bearing that is 0.1 N, 0.2 N, 0.3 N, 0.4 N, 0.5 N, and 0.6 N. Bearing with the first embodiment was tested for motion stability at rotational speed of 10,560 rpm while the second embodiment of the bearing was tried at the speed of

13,275 rpm. Figure 14 shows experimentally measured motion stability of the bearing in its first embodiment.

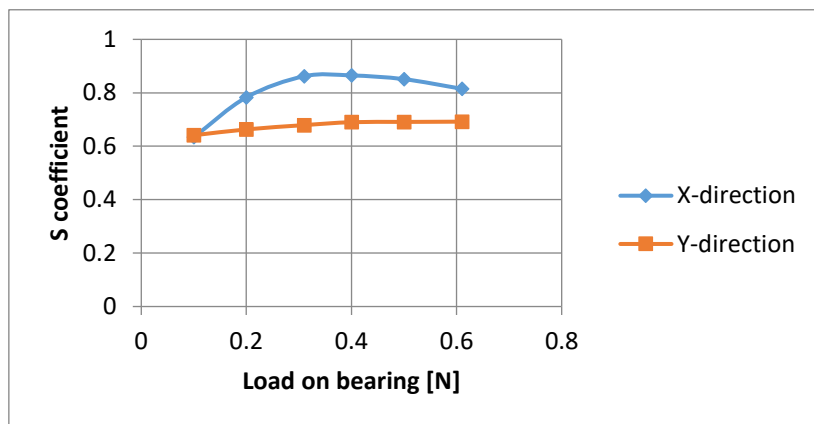


Figure 14

Change in the magnitude of stability coefficient, S , as a function of load on the bearing in its first embodiment.

The frequency of elastic deformation of the bearing induced by PZTs was 78.8 kHz and corresponded to a resonance frequency as estimated by modal analysis. Beneficial effect of squeeze film pressure generated by PZTs is clearly visible. At the lowest load on bearing (0.1 N) switching PZTs on resulted in almost 35% reduction of shaft motion because $S = 0.634$ for X-direction and $S = 0.641$ for Y-direction. However with increase in the load on bearing the effectiveness of PZTs action, as measured by values of S coefficient in X and Y direction is diminishing. The reason for that is undoubtedly stabilising effect of increase in the load acting on the bearing. Figure 15 depicts results for the second embodiment of the bearing.

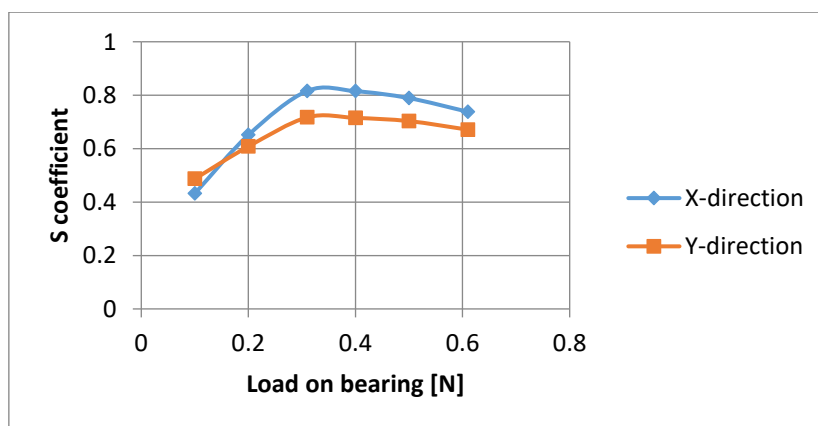


Figure 15

Change in the magnitude of stability coefficient, S , as a function of load on the bearing in its second embodiment

This bearing is characterised by enhanced flexibility due to the use of “elastic hinges”. Therefore, its resonance frequency was only 8.8 kHz. At the lightest load (increased propensity to run unstable) the effect of switching on PZTs on the reduction of shaft’s motion is unquestionable. The S coefficient in X and Y directions is 0.432 and 0.487 respectively which means more than 50% reduction of the shaft’s motion. At the load on bearing equal to 0.31 N the reduction of shaft motion as measured by the magnitude of S coefficients is much less comparing to the previous load as S coefficient for X and Y direction is 0.816 and 0.717 respectively. This is a clear confirmation of the fact that an air bearing becomes more stable when the load on it is increased. At the highest load on the bearing used (0.62 N) the S coefficient in X and Y direction is 0.738 and 0.671 respectively, which is slightly lower than that recorded for load of 0.31 N. This can be explained by the effect of the offset deformation of the bearing shell transforming a circular bore into three lobe geometry, which is known to have a stabilising effect on its own.

6.3 Assessment of embodiment effect on performance

There is no doubt that the bearing with increased flexibility (second embodiment) is superior in all aspects of performance comparing to that shown by the bearing without built-in flexibility (first embodiment). This conclusion is based on experimental test results accounting for the performance of two types of bearing tested and the ranking is based entirely on them. Bearing with the second embodiment is able to deform elastically much more than the bearing with the first embodiment. Therefore, in a deformed shape the three lobe geometry of the bore is far more pronounced for the bearing with second embodiment than it is the case for the bearing’s first embodiment. Larger elastic deformation of the bearing with second embodiment also facilitates squeeze film action much more effectively. However, it is necessary to remember practicalities concerning machining of the bearing and associated problems. Undoubtedly, second embodiment represents far more complicated geometry and, hence, problems with its machining. Furthermore, elastic hinges providing enhanced flexibility are a potential source of fatigue cracks, which in a long run operation of the bearing, might be of significant importance. This practical aspect awaits additional studies and assessment.

7. Conclusions

Results presented in this paper permit the following conclusions.

1. Overall flexibility of the bearing’s shell plays an important role in the performance of an acoustic journal bearing operating on the squeeze film acoustic levitation principle. More flexible is the bearing’s shell the better performance is exhibited by the bearing judging by the results of experimental testing.
2. Although performance of the bearing with the second embodiment proved to be far superior to that of the bearing with first embodiment, nevertheless practical considerations such as complex machining and fatigue endurance create some doubts concerning advantages and benefits.

Acknowledgements

Some of the results presented in this paper were generated within the project supported by the grant from the National Centre of Science, Poland, (grant no.: 2012/07/B/ST8/03683).

References

- [1] Wardle, F., 2015, *Ultra-precision Bearings*, Woodhead Publishing, London
- [2] Mizumoto, H., Arii, S., Yabuta, Y., Kami, Y., Tazoe, Y., 2007, "Active Aerostatic Bearings for Ultraprecision Applications", *Proceedings of the 35th International MATADOR Conference*, Springer, London.
- [3] Matsumura, F., Okada, Y., Fujita, M., Namerikawa, T., 1997, "State of the Art of Magnetic Bearings: Overview of Magnetic Bearing Research and Applications", *JSME Intern.J Series C*, 40, pp. 553-560.
- [4] Langois, W., 1962, "Isothermal squeeze films", *Quarterly of Applied Mathematics*, 20, pp. 131-150.
- [5] Hashimoto, Y., Yoshikazu, K., and Sadayuki, U., 1998, "Transporting objects without contact using flexural traveling waves", *The Journal of the Acoustical Society of America*, 103, pp. 3230-3233.
- [6] Matsuo, E., 2000, "Holding characteristics of planar objects suspended by near-field acoustic levitation", *Ultrasonics*, 38, pp. 60-63.
- [7] Ueha, S., Yoshiki, H., and K. Yoshikazu, K., 2000, "Non-contact transportation using near-field acoustic levitation", *Ultrasonics*, 38, pp. 26-32.
- [8] Minikes, A., and Izhak, B., 2003, "Coupled dynamics of a squeeze-film levitated mass and a vibrating piezoelectric disc: numerical analysis and experimental study", *J Sound and Vibration*, 263, pp. 241-268.
- [9] Nomura, H., Kamakura, T., 2002, "Theoretical and experimental examination of near-field acoustic levitation", *The Journal of Acoustical Society of America*, 111, pp. 1578-1584.
- [10] Hu, J., Li, G., Chan, H.L.W., and Choy, C.L., 2001, "A standing wave-type noncontact linear ultrasonic motor", *IEEE Transactions on Ultrasonics, Ferroelectrics, and Frequency Control*, 48, pp. 699-708.
- [11] Foresti, D., Nabavi, M., Klingauf, M., Ferrari, A., Poulidakos, D., 2013, "Acoustophoretic contactless transport and handling of matter in air", *Proc. National Academy of Sciences of USA*, 110, pp. 12549 – 12554.
- [12] Stolarski, T.A., Woolliscroft, C., 2007, "Use of near-field acoustic levitation in experimental sliding contact", *J Appl. Mech.*, 74, pp. 816-820.
- [13] Wang, Y.Z., Wei, B., 2013, "Mixed-modal disk gas squeeze film theoretical and experimental analysis", *International Journal of Modern Physics, B*, 27, pp. 1-20.

- [14] Ilssar, D., Bucher, I., Cohen, N., 2014, "Structural optimization for one dimensional acoustic levitation devices – Numerical and experimental study", 2014, Proc. Int. Conf. Noise Vib. Eng., (ISMAB 2014), Leuven, Belgium.
- [15] Ilssar, D., Bucher, I., 2015, "On the slow dynamics of near-field acoustically levitated objects under High excitation frequencies", J. Sound and Vibration, 354, pp. 154–166.
- [16] Chang, X., Wei, B., Atherton, M., Mares, C., Stolarski, T.A., Almurshedi, A., 2016, "NFAL Prototype Design and Feasibility Analysis for Self-Levitated Conveying", Tribology Transactions, 59, pp. 957-968.
- [17] Wei, B., Shaham, R. and Bucher, I., 2018, "Theoretical investigation and prototype design for non-parallel squeeze film movement platform driven by standing waves", Tribology International, 119, pp. 539 – 548.
- [18] Stolarski, T.A. and Wei Chai, 2006, "Load-carrying capacity generation in squeeze film action", Int. J. Mech. Sci., 48, pp. 736-741.